第 30 卷 第 5 期　　力　学　学　报　　Vol. 30 ,No. 5
1998 年 9 月　　ACTA MECHANICA SINICA　　Sept. , 1998

高速三维边界层的横流不稳定性[1)]

赵耕夫　徐　立

(天津大学力学系, 天津 300072)

摘要　用两点四阶差分格式研究旋转圆锥超音速三维边界层的横流不稳定性和壁面冷却对稳定性的影响. 数值结果表明,与二维边界层相比横流使三维边界层第一模式增长率增大,对第二模式影响很小; $M_e < 4.3$ 第一模式最不稳定, $M_e > 4.3$ 第二模式最不稳定;三维边界层最不稳定第二模式是三维波,二维边界层则为二维波;壁面冷却对第一模式起稳定作用,对第二模式起不稳定作用.

关键词　超音速流,高超音速流,三维边界层,横流不稳定性,壁面冷却

引　言

后掠翼三维边界层具有多种失稳机制,其中横流不稳定性起主导作用,是研究三维边界层的焦点. 由于实验研究还不充分,至今人们对三维边界层失稳机理的认识还不深入,已有的结果也不尽一致,仍有一些亟待解决的问题[1]. 可压缩性对横流不稳定性的影响就是需要深入研究的问题. 本文将详细讨论超音速、高超音速三维边界层的横流不稳定性.

Kobayashi 等通过实验及理论分析绕旋转圆锥的不可压缩流动,证明所得的结果可以直接应用于后掠翼三维边界层[2,3]. 就高速后掠翼而言,即便平均流的计算也是困难问题,因此旋转圆锥是研究高速三维边界层横流不稳定性的最合适的模型. 影响可压缩边界层稳定性数值结果的重要因素是数值方法及热力学参数的合理近似. 本文将 Mack 的四阶精度紧密差分格式用于求解超音速、高超音速的稳定性问题,最大马赫数为 8[4]. 考虑到高速边界层内温度变化很大,放弃了可压缩稳定性分析传统方式(粘性系数 Suthland 公式、常数普朗特数和等压比热),而直接用高阶多项式拟合空气热力学参数实验数据[5].

1　三维边界层平均流

均匀超音速流流过零攻角旋转圆锥,半锥角 $\theta = 15°$,旋转角速度 Ω. 如图 1 所示, ξ 为流向坐标, ζ 指向锥面垂直方向, η 为圆周方向坐标. 设 U, V, W 为 ξ, ζ, η 方向的速度分量,经过 Mangler 变换后速度为 $\overline{U} = U$, $\widetilde{W} = W$, $\overline{V} = \frac{L}{r}\left(V + \frac{\mathrm{d}r}{\mathrm{d}\xi}\frac{1}{r}\zeta U\right)$,当 $\Omega \neq 0$ 时经变换的方程无相似

---

1) 国家自然科学基金资助项目(19372038).

1996 - 10 - 24 收到第一稿, 1998 - 01 - 08 收到修改稿.

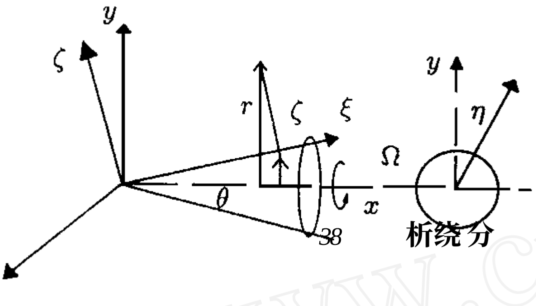

图 1 坐标系

Fig. 1 Coordinate axis

解,为减少方程对 M_e 数、壁面及外缘温度 T_w, T_e 及其他可变参数的依赖,取 Falknar - Scan 变换的可压缩形式

$$\left.\begin{aligned} ds &= \left(\frac{\rho_e U_e}{\mu_e x}\right)^{1/2}\frac{\rho}{\rho_e}dy, \\ \psi(x, y) &= (\rho_e\mu_e U_e x)^{1/2} f(x, s) \end{aligned}\right\} \tag{1.2}$$

4 .3

式中 $\rho_e\mu_e U_e h_e$ 为边界层外缘的密度、粘性系数、流向速度和焓, $w(x, s)$, $g(x, s)$ 分别是无量纲的周向速度分量和比焓. 取 $L = 1$,利用上式三维可压缩边界层方程变为

$$(bf'')' + m_1 ff'' + m_2(g - f'^2) + \frac{w^2}{3} = x\left(f'\frac{\partial f'}{\partial x} - f''\frac{\partial f}{\partial x}\right) \tag{1.3}$$

$$(bw')' + m_1 fw' - m_3 f'w = x\left(f'\frac{\partial w}{\partial x} - w'\frac{\partial f}{\partial x}\right) \tag{1.4}$$

$$(eg')' + m_1 C_p fg' + (\gamma - 1) M_e^2 b(f''^2 + w'^2) = xC_p\left(f'\frac{\partial g}{\partial x} - g'\frac{\partial f}{\partial x}\right) \tag{1.5}$$

式中, C_p 为等压比热, M_e 是边界层外边界处的马赫数,边界条件为

$$s = 0, \quad f' = f = 0, \quad w = \frac{\Omega}{U_e}(3\sin\theta)^{1/3}, \quad g' = 0 \text{ 或 } g = h_w/h_e \tag{1.6}$$

$$s = s_e, \quad f' = 1, \quad w = 0, \quad g = 1.$$

参数 $b = \dfrac{\rho\mu}{\rho_e\mu_e}$, $m_1 = \dfrac{1}{2}\left(1 + \dfrac{x}{\rho_e\mu_e}\dfrac{d(\rho_e\mu_e)}{dx} + m_2\right)$, $m_2 = \dfrac{x}{U_e}\dfrac{dU_e}{dx}$, $m_3 = m_2 + 1/3$, $e = bC_p/Pr$. 本文用盒式方法求解方程(1.3)~(1.6) [6].

2 扰动方程

考虑平均流对无限小扰动的线性稳定性. 为此在平均流 q_s 上叠加上小扰动 q',则瞬时速度流场可表示为

$$q(\xi, \zeta, \eta, t) = q_s(\zeta) + q'(\xi, \zeta, \eta, t) \tag{2.1}$$

其中 $q_s = (u_s, w_s, T, p)$ 为平均流, $q' = (u', v', w', \tau', p')$ 为无限小扰动. 假定空气是完全气体,处于平衡态,粘性系数 μ 和热传导系数 k 只是温度的函数. 温度扰动量是无限小量,粘性系数可展成

$$\mu = \mu_s + \frac{d\mu_s}{dT}\tau' \tag{2.2}$$

以边界层外缘参数 $U_e, \rho_e, T_e, \mu_e, k_e, C_{p_e}$ 及特征长度 $\delta = \sqrt{\frac{V_e \xi}{U_e}}$ 使各参数无量纲化．根据局部平行流假定，小扰动 q 可表示成

$$q' = \Phi(\zeta)\exp[i(\alpha\xi + m\eta - \omega t)] + c.c. \tag{2.3}$$

其中 c.c. 表示共轭，α, m 分别为流向和周向波数，ω 为频率．时间模式 α, m 为实数，ω 为复数，ω_r 是扰动频率，ω_i 是扰动的时间增长率．空间模式 ω, m 为实数，α 为复数，$-\alpha_i$ 是扰动沿流向的增长率．本文只计算时间模式问题．把(2.1)～(2.3)代入无量纲三维 Navier - Stokes 方程并减去平均流方程后得如下小扰动分方程

$$(AD^2 + BD + C)\Phi = 0 \tag{2.4}$$

边界条件为[7]

$$\left.\begin{aligned} \zeta = 0, \quad & \tilde{u} = \tilde{v} = \overline{w} = \tilde{\tau} = 0 \\ \zeta \to \infty, \quad & \tilde{u} = \tilde{v} = \overline{w} = \tilde{\tau} = 0 \end{aligned}\right\}$$

方向的夹角 $\theta_p = \tan^{-1}(W_p)$,按稳定性的定义横流指向势流的垂直方向. 在此坐标系中横流速度分量为

$$Q = (w_p - w)\cos\theta_p - U\sin\theta_p \tag{3.1}$$

首先考察了空气热力学参数的不同近似对扰动增长率的影响. $T_e = 200$, $M_e = 3$ 时本文方法和传统方法得到的最大增长率相对误差 1 %,若 $T_e = 70$, $M_e = 3$ 两者相比误差 13.2 %, $M_e = 5$ 时则为 19.8 %. 势流温度越低, M_e 数越大,相对误差越大.

为了研究三维、二维边界层不同的稳定性机理,我们在横流方向叠加一均匀流来消除横流分量,以便于比较有无横流两种情况的稳定性. 这一新速度在流向和周向的分量为

$$U_c = (U\cos\theta_p - W\sin\theta_p)\cos\theta_p + \sin^2\theta_p \tag{3.2}$$

$$W_c = -(U\cos\theta_p - W\sin\theta_p)\sin\theta_p + \cos\theta_p\sin\theta_p \tag{3.3}$$

图 2 为有横流和无横流时不同波角扰动的时间增长率与流向波数的函数关系,其中波角 $\phi = \tan^{-1}(\beta/\alpha)$, $\beta = m/r$ (若 $\Omega = 375$,在动坐标系中势流与流向的夹角为 $-16.2°$,波矢与势流的夹角 $\theta_m = \phi + 16.2$). 显然有横流时扰动的增长率比无横流情况大得多,两者最大增长率之比为 2.46. 图 3 为 $M_e = 2$, $Re = 600$ 有横流时增长率与频率的关系. 横流在很宽的频带内是不稳定的,无横流的不稳定频带要窄得多. 表明定常波和行进波同时存在,且行进波比定常波更不稳定,最不稳定定常波与势流的夹角为 88°,高速边界层并未改变横流的基本性质[8].

图4为 $M_e = 5$, $Re = 3000$有无横流两种情况增长率和波数的函数关系. 在此 M_e数两种

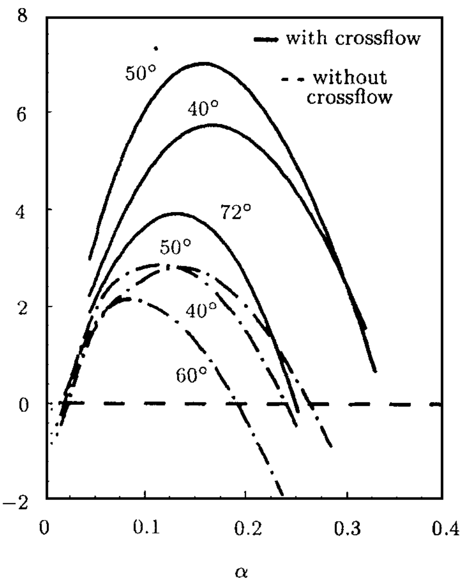

图 2　有横流和无横流扰动增长率比较

$M_e = 3$, $Re = 3000$

Fig. 2　Comparison of growth rates with crossflow and without crossflow　$M_e = 3$, $Re = 3000$

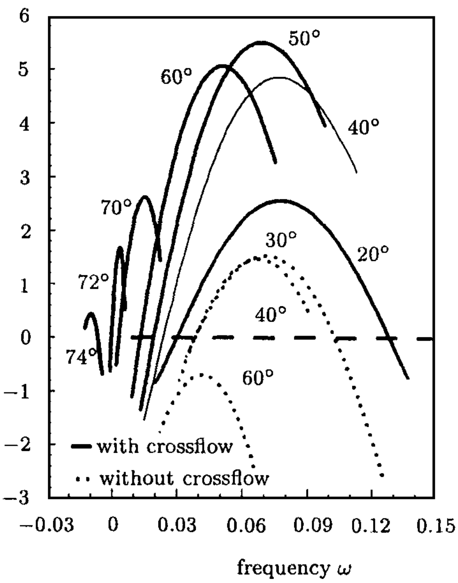

图 3　有横流时增长率与频率的关系

$M_e = 2$, $Re = 600$

Fig. 3　Growth rates vs. frequency with crossflow at　$M_e = 2$, $Re = 600$

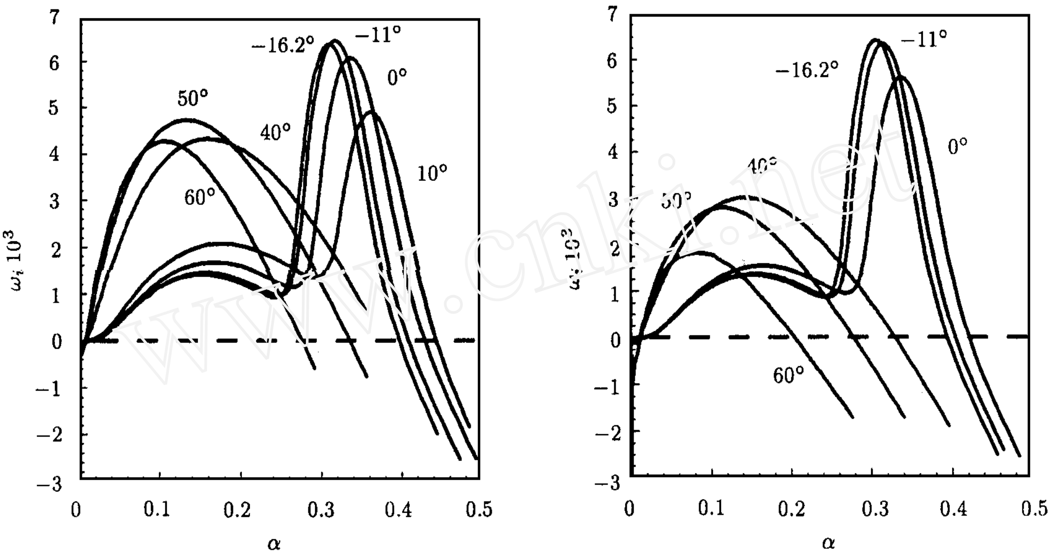

(a) 有横流

(a) with crossflow

(b) 无横流

(b) without crossflow

图 4　扰动增长率和波数的关系 $M_e = 5$, $Re = 3000$

Fig. 4　Growth rates vs wavenumber $M_e = 5$, $Re = 3000$

情况都出现了第二模式,第二模式的增长率大于第一模式. 无横流最不稳定第二模式与势流方向的夹角为零度,是二维波. 但有横流最不稳定第二模式与势流夹角为 5°,是三维波,这是三维边界层不同于二维的又一特点. 表 1 给出 $M_e = 5$, $Re = 600$, 2000, 3000 有无横流两种情况最大增长率及相应的波角. 有横流和无横流第一模式最大增长率之比分别为 2.05, 1.63, 1.58. 第二模式最大增长率之比为 0.62, 1.0, 1.0,显然横流对第二模式影响很小. 从表 1 可以看出扰动增长率随雷诺数的增大而增大,表明了粘性的稳定作用,这是可压缩稳定性与不可压缩情况的重要区别.

表 1　不同雷诺数的最大增长率及其波角

Table 1　The Maximal growth rate and phase angle at different Reynolds numbers

(a) with crossflow					(b) without crossflow				
	The first mode		The second mode			The first mode		The second mode	
Re	θ_m	ω_{im}	θ_m	ω_{im}	Re	θ_m	ω_{im}	θ_m	ω_{im}
600	66	0.00271	5	0.00287	600	60	0.00132	0	0.00462
2000	66	0.00441	5	0.00581	2000	56	0.00271	0	0.00580
3000	67	0.00473	5	0.00645	3000	56	0.00300	0	0.00643

图 5 为 $M_e = 8$ 有无横流两种情况的增长率曲线. 有横流时最不稳定第二模式与势流方向的夹角为 9.5°,无横流则为 0°. 有横流和无横流第一、二模式最大增长率之比分别为 1.33, 1.02. 以上比值表明横流对第一模式增长率的影响随着 M_e 数的增大而减弱. 横流虽然使第一模式增长率增大,但仍小于第二模式. 图 6 显示了 $Re = 3000$ 扰动的最大增长率随 M_e 数的变化. 第一模式 $M_e = 2$ 时达最大值,然后随 M_e 数增大而逐渐减小. 第二模式 $M_e = 5$ 时增长率达

最大值 ,随后迅速减小 . 证明了可压缩性不管对第一模式还是第二模式都有较强的稳定作用 . 同时也表明 M_e 数小于 4.3 时第一模式最不稳定 ,更高 M_e 数则第二模式起主导作用 .

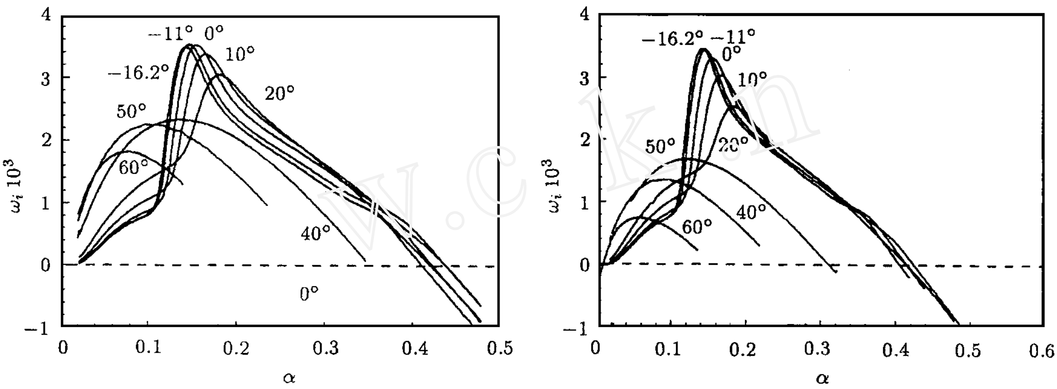

(a) 有横流
(a) with crossflow

(b) 无横流
(b) without crossflow

图 5　扰动增长率和波数的关系 $M_e = 8$, $Re = 3000$

Fig. 5　Growth rates vs wavenumber $M_e = 8$, $Re = 3000$

图 7 所示为壁面冷却对增长率的影响($Re = 3000$, $M_e = 5$,相应于最不稳定波) . 壁面温度降低第一模式的增长率减小 ,第二模式增长率增大 ,其最不稳定频率升高 . 证明三维边界层和二维边界层一样 ,壁面冷却只对第一模式有稳定作用 ,对第二模式则起不稳定作用[9] .

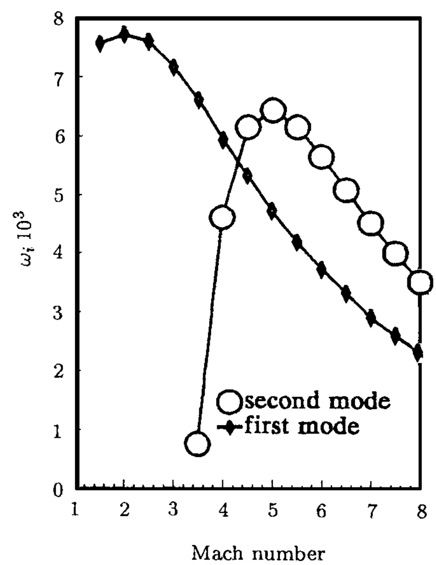

图 6　扰动最大增长率和 M_e 的关系

Fig. 6　Maximum growth rates vs. Mach number at $Re = 3000$

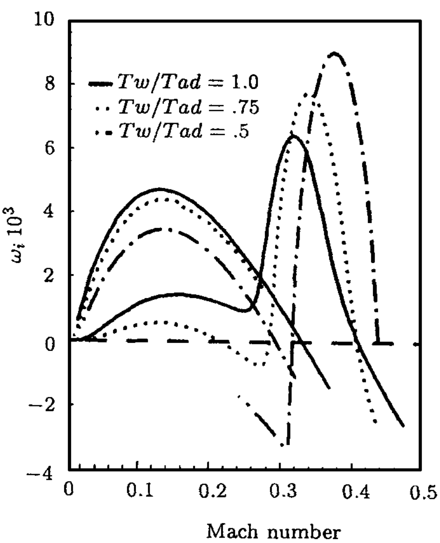

图 7　壁面冷却对增长率的影响 $M_e = 5$, $Re = 3000$

Fig. 7　Effect of the wall cooling on the growth rates at $M_e = 5$, $Re = 3000$

4　结　论

本文数值方法分析了旋转圆锥高速三维边界层的横流不稳定性和壁面冷却对横流稳定性的影响．数值结果证明，在三维边界层中 $M_e < 4.3$ 时最不稳定的是第一模式的扰动，$M_e > 4.3$ 最不稳定的是第二模式．三维边界层和具有相同势流方向速度剖面的二维边界层相比，第一模式增长率增大，但横流对第一模式的影响随着 M_e 数的增大而减弱．横流对第二模式的 增长率影响很小．数值结果还证明三维边界层最不稳定的第二模式是三维波，二维边界层最不稳定第二模式是二维波．三维边界层在很宽频率带内存在横流不稳定性，定常波行进波同时存在，且行进波比定常波更不稳定．本文证明壁面冷却对高速三维边界层的第一模式有较强的稳定作用，对第二模式则起不稳定作用．

参　考　文　献

1　Reed HL, Saric WS. Stability of three - dimensional boundary layers. *Ann Rev Fluid Mech*, 1989, 21: 235～284

2　Kobayashi R, Kohana Y, Kurosawa M. Boundary layer transition on a rotating cone in axial flow. *J Fluid Mech*, 1983, 127:341～352

3　Kobayashi R, Izumi H. Boundary layer transition on a rotating cone in still fluid. *J Fluid Mech*, 1983, 127: 353～364

4　Malik MR, Chuang S, Hussaini M, Angew Z. Accurate numerical solution of a compressible linear stability equation. *Math Phys*, 1982 33: 189～201

5　赵耕夫．空气热力学参数对可压缩边界层线性稳定性的影响．空气动力学学报，1996, 14(1): 98～103 (Zhao Gengfu. The effects of thermodynamic parameters of air on the instability of compressible boundary layer flow. *Acta Aerodynamica Sinica*, 1996, 14(1): 98～103 (in Chinese))

6　Cebeci T, Bradshaw P. 对流传热的物理特性及计算．北京：清华大学出版社，朱自强译, 1988. (Cebeci T, Bradshaw P. Physical and Computational Aspects of Convective Heat Transfer. Beijing: Qinghua University Press, translated by Zhu Ziqiang, 1988 (in Chinese))

7　赵耕夫．论可压缩平板边界层线性稳定性的分歧．力学学报, 1997, 29(1):24～29 (Zhao Gengfu. On the dispute with regard to viscous linear stability of compressible boundary layer. *Acta Mechanica Sinica*, 1997, 29(1):24～29 (in Chinese))

8　Nitchke - Kowsky P, Bippes H. Instability and transition of a three - dimensional boundary layer on a swept flat plate. *Phys. Fluids*, 1988, 32(4): 786～795.

9　Mack LM. Reviev of linear compressible stability theory. In:Dwoyer DL & Hissuini UY, ed. Stability of Time - Dependent and Spatial Varying Flows. New York: Springer - Verlag, 1985. 164～187

附录

$$A_{11} = A_{22} = A_{33} = A_{44} = B_{52} = 1.0$$

$$B_{11} = B_{22} = B_{33} = \frac{\cos\theta}{r} + \frac{1}{\mu_s}\frac{\mathrm{d}\mu_s}{\mathrm{d}T}\frac{\mathrm{d}T_s}{\mathrm{d}\zeta}, \quad B_{12} = \frac{\mathrm{i}\alpha}{3}, \quad B_{14} = \frac{1}{\mu_s}\frac{\mathrm{d}\mu_s}{\mathrm{d}T}\frac{\mathrm{d}u_s}{\mathrm{d}\zeta}$$

$$B_{21} = \frac{\mathrm{i}\alpha}{4} + \frac{\sin\theta}{4r}, \quad B_{23} = \frac{\mathrm{i}m}{4r}, \quad B_{24} = -\frac{1}{\mu_s}\frac{\mathrm{d}\mu_s}{\mathrm{d}T}\frac{u_s\sin\theta}{2r}, \quad B_{25} = -\frac{3Re}{4\mu_s}$$

$$B_{32} = \frac{\mathrm{i}m}{3r}, \quad B_{34} = \frac{1}{\mu_s}\frac{\mathrm{d}\mu_s}{\mathrm{d}T}\text{表面}\left(\frac{\mathrm{d}w_s}{\mathrm{d}\zeta} - \frac{w_s\cos\theta}{r}\right., \quad B_{41} = 2Pr(\gamma - 1)M_e^2\frac{\mu_s}{k_s}\frac{\mathrm{d}u_s}{\mathrm{d}\zeta}$$

$$B_{42} = -\frac{4}{3} Pr(\gamma - 1) M_e^2 \frac{\mu_s u_s \sin\theta}{k_s r}, \quad B_{43} = 2 Pr(\gamma - 1) M_e^2 \frac{\mu_s}{k_s}\left(\frac{d w_s}{d\zeta} - \frac{w_s \cos\theta}{r}\right)$$

$$B_{44} = \frac{2}{\mu_s}\frac{d\mu_s}{dT}\frac{dT_s}{d\zeta} + \frac{\cos\theta}{r}$$

$$C_{11} = \frac{4}{3}\left(\frac{i\alpha}{r}\sin\theta - \frac{\sin^2\theta}{r^2} - \alpha^2 - \frac{m^2}{r^2} - \frac{Re}{\mu_s} i\rho_s\left(\alpha u_s + \frac{m}{r} w_s - \omega\right)\right)$$

$$C_{12} = \frac{i\alpha}{3r}\cos\theta - \frac{4}{3r^2}\sin\theta\cos\theta + \frac{i\alpha}{\mu_s}\frac{d\mu_s}{dT}\frac{dT_s}{d\zeta} - \frac{Re}{\mu_s}\rho_s\frac{du_s}{d\zeta}$$

$$C_{13} = -\frac{\alpha m}{3r} - \frac{7im}{3r^2}\sin\theta + \frac{2Re}{\mu_s}\frac{\rho_s w_s}{r}\sin\theta$$

$$C_{14} = \frac{1}{\mu_s}\frac{d^2\mu_s}{dT^2}\frac{dT_s}{d\zeta}\frac{du_s}{d\zeta} + \frac{1}{\mu_s}\frac{d\mu_s}{dT}\left(\frac{d^2u_s}{d\zeta^2} - \frac{4u_s}{3r^2}\sin^2\theta - \frac{2i\alpha}{3r}u_s\sin\theta - \right.$$
$$\left. - \frac{Re}{\mu_s}\frac{w_s^2}{r}\frac{\rho_s}{T_s}\sin\theta\right)$$

$$C_{15} = \gamma M_e^2\frac{Re}{\mu_s}\frac{\rho_s w_s^2}{r}\sin\theta - \frac{Re}{\mu_s} i\alpha$$

$$C_{21} = -\frac{1}{\mu_s}\frac{d\mu_s}{dT}\frac{dT_s}{d\zeta}\left(\frac{i\alpha}{2} + \frac{\sin\theta}{2r} - \frac{\sin\theta\cos\theta}{r^2}\right)$$

$$C_{22} = \frac{3i\alpha\sin\theta}{4r} - \frac{3}{4}\left(\alpha^2 + \frac{m^2}{r^2} - \frac{1}{\mu_s}\frac{d\mu_s}{dT}\frac{dT_s}{d\zeta}\frac{\cos\theta}{2r} - \frac{\cos^2\theta}{r^2} - \right.$$
$$\left. \frac{3i\rho_s Re}{4\mu_s}\left(\alpha u_s + \frac{m}{r}w_s - \omega\right)\right)$$

$$C_{23} = -\frac{1}{\mu_s}\frac{d\mu_s}{dT}\frac{dT_s}{d\zeta}\frac{im}{2r} - \frac{7im\cos\theta}{4r^2} + \frac{3}{2}\frac{Re}{\mu_s}\frac{\rho_s w_s\cos\theta}{r}$$

$$C_{24} = \frac{1}{\mu_s}\frac{d\mu_s}{dT}\left[\frac{du_s}{d\zeta}\frac{\sin\theta}{4r} + \frac{3i\alpha}{4}\frac{du_s}{d\zeta} - \frac{u_s\sin\theta\cos\theta}{r^2} + \right.$$
$$\left. - \frac{1}{\mu_s}\frac{d^2\mu_s}{dT^2}\frac{dT_s}{d\zeta}\frac{u_s\sin\theta}{2r} - \frac{3}{4}\frac{Re}{\mu_s}\frac{w_s^2\cos\theta}{r}\frac{\rho_s}{T_s}\right]$$

$$C_{25} = \frac{3}{4}\gamma M_e^2\frac{Re}{\mu_s}\frac{\rho_s w_s^2\cos\theta}{r}, \quad C_{31} = -\frac{Re}{\mu_s}\frac{\rho_s w_s\sin\theta}{r} - \frac{\alpha m}{3r} + \frac{7im\sin\theta}{3r^2}$$

$$C_{32} = -\frac{Re\rho_s}{\mu_s}\left(\frac{dw_s}{d\zeta} + \frac{w_s}{r}\cos\theta\right) + \frac{1}{\mu_s}\frac{d\mu_s}{dT}\frac{dT_s}{d\zeta}\frac{im}{r} + \frac{7im\cos\theta}{3r^2}$$

$$C_{33} = -\frac{Re}{\mu_s}\left[i\rho_s\left(\alpha u_s + \frac{m}{r}w_s - \omega\right) + \frac{\rho_s\mu_s\sin\theta}{r}\right] - \alpha^2 - \frac{1}{r^2} + \frac{i\alpha\sin\theta}{r} - $$
$$\frac{4m^2}{3r^2} - \frac{1}{\mu_s}\frac{d\mu_s}{dT}\frac{dT_s}{d\zeta}\frac{\cos\theta}{r}$$

$$C_{34} = -\frac{1}{\mu_s}\frac{d\mu_s}{dT}\left(\frac{i\alpha}{r}w_s\sin\theta - \frac{4im}{3r^2}u_s\sin\theta - \frac{dw_s}{d\zeta}\frac{\cos\theta}{r} + \frac{w_s}{r^2} + \frac{d^2w_s}{d\zeta^2} + \right.$$

$$\frac{1}{\mu_s}\frac{\mathrm{d}^2\mu_s}{\mathrm{d}T^2}\frac{\mathrm{d}T_s}{\mathrm{d}\zeta}\left(\frac{\mathrm{d}w_s}{\mathrm{d}\zeta}-\frac{w_s\cos\theta}{r}\right)+\frac{Re}{\mu_s}\frac{u_s w_s\sin\theta}{r}\left(\frac{\rho_s}{T_s}\right)$$

$$C_{35}=-\frac{Re}{\mu_s}\left(\gamma M_e^2\frac{u_s w_s}{rT_s}\sin\theta+\frac{\mathrm{i}m}{r}\right)$$

$$C_{41}=Pr(\gamma-1)M_e^2\frac{\mu_s}{k_s}\left(-\frac{4\mathrm{i}\alpha u_s}{3r}+\frac{8u_s}{3r^2}\sin\theta-\frac{2\mathrm{i}mw_s}{r^2}\right)\sin\theta$$

$$C_{42}=Pr(\gamma-1)M_e^2\frac{\mu_s}{k_s}\left(2\mathrm{i}\alpha\frac{\mathrm{d}u_s}{\mathrm{d}\zeta}+\frac{4u_s}{3r^2}\sin2\theta+\frac{2\mathrm{i}m}{r}\frac{\mathrm{d}w_s}{\mathrm{d}\zeta}-\frac{2\mathrm{i}mw_s}{r^2}\cos\theta\right)-\frac{PrRe}{\mu_s}\rho_s\frac{\mathrm{d}T_s}{\mathrm{d}\zeta}$$

$$C_{43}=Pr(\gamma-1)M_e^2\frac{\mu_s}{k_s}\left(-\frac{2\mathrm{i}\alpha w_s}{r}\sin\theta+\frac{2w_s}{r^2}+\frac{8\mathrm{i}mu_s}{3r^2}\sin\theta-\frac{\mathrm{d}w_s}{\mathrm{d}\zeta}\frac{2\cos\theta}{r}\right)$$

$$C_{44}=\frac{1}{\mu_s}\frac{\mathrm{d}\mu_s}{\mathrm{d}T}\left(\frac{\mathrm{d}^2T_s}{\mathrm{d}\zeta^2}+\frac{\mathrm{d}T_s}{\mathrm{d}\zeta}\frac{\cos\theta}{r}\right)+\frac{1}{\mu_s}\frac{\mathrm{d}^2\mu_s}{\mathrm{d}T^2}\left(\frac{\mathrm{d}T_s}{\mathrm{d}\zeta}\right)^2-\alpha^2-\frac{m^2}{r^2}+$$
$$\frac{\mathrm{i}\alpha}{r}\sin\theta+Pr(\gamma-1)M_e^2\frac{1}{k_s}\frac{\mathrm{d}\mu_s}{\mathrm{d}T}\left[\left(\frac{\mathrm{d}u_s}{\mathrm{d}\zeta}\right)^2+\left(\frac{\mathrm{d}w_s}{\mathrm{d}\zeta}\right)^2+\frac{w_s^2}{r^2}\right]-$$
$$\frac{\mathrm{i}PrRe\rho_s}{k_s}\left(\alpha u_s+\frac{m}{r}w_s-\omega\right)$$

$$C_{45}=Pr(\gamma-1)M_e^2\frac{Re}{\mu_s}\mathrm{i}\left(\alpha u_s+\frac{mw_s}{r}-\omega\right),\quad C_{51}=\mathrm{i}\alpha+\frac{\sin\theta}{r}$$

$$C_{52}=\frac{\cos\theta}{r}+\frac{1}{\rho_s}\frac{\mathrm{d}\rho_s}{\mathrm{d}\zeta},\quad C_{53}=\frac{\mathrm{i}m}{r},\quad C_{54}=-\mathrm{i}\rho_s\left(\alpha u_s+\frac{mw_s}{r}-\omega\right)-\frac{\rho_s u_s\sin\theta}{r}$$

$$C_{55}=\gamma M_e^2\left[\mathrm{i}\left(\alpha u_s+\frac{mw_s}{r}-\omega\right)+\frac{u_s\sin\theta}{r}\right]$$

CROSSFLOW INSTABILITY OF HIGH SPEED THREE-DIMENSIONAL BOUNDARY LAYER[1)]

Zhao Gengfu Xu Li

(Department of Mechanics, Tianjin University. Tianjin 300072, China)

Abstract There exist variety of instability in three dimensional boundary layer on swept wing, the cross-flow instability is dominant. The flow over rotating cone is typical three dimensional boundary layer. It has been shown that the experimental and theoretical results of rotating cone can be used to model cross flow instability of swept wing. At high speeds, where even the basic flow calculations of swept wing are a problem, owe to it's simple geometry, rotating cone become a suitable and valuable model to study cross flow instability of high speed three dimensional boundary layer on swept wing. In this paper, a rotating sharp cone which located in a supersonic/hypersonic free stream at zero attack is used as a model to study the cross flow instability of high speed three dimensional boundary layer. The purpose of present work is to investigate the different instability mechanism of two and three dimensional boundary layers and effect of wall cooling on the instability. The basic boundary layer flow is calculated using box scheme and the instability eigenvalue problem is solved by a fourth-order accurate two-point finite difference scheme. Since the calssical approximation method of thermodynamic parameters of the air has not enough accuracy for numerical analysis of high speed instability problem, a high degree polynomial is used to imitate the dependence on temperature of viscosity, conductivity, Prandtl number and specific heat from experimental data.

The numerical results show that the growth rates of cross-flow first mode are larger comparing with those in two-dimensional case and the influence of cross flow decreases as Mach number increases but the influence of cross-flow on the second mode is weakly. The results also show that the instability with cross flow cover a much wider range of unstable frequencies than those without cross flow and the growth rates of travelling waves are larger than stationary waves, the most unstable stationary wave is approximately perpendicular to potential flow direction. If $M_e < 4.3$ the most unstable disturbance is the first mode, if $M_e > 4.3$ it is the second mode. In three dimensional boundary layer the most unstable second mode is oblique, in two dimensional boundary layer is two-dimensiona; Cooling the wall stabilizes the first mode, destabilizes the second mode.

Key words supersonic flow, hypersonic flow, 3D boundary layer, cross-flow instability, wall cooling

1) The project supported by the National Natural Science Foundation of China

Received 24 October 1996, revised 8 January 1998.